Available online at www.sciencedirect.com
SCIENCE DIRECT®
European Polymer Journal 40 (2004) 965–974
EUROPEAN POLYMER JOURNAL
www.elsevier.com/locate/europolj

In situ estimation of the chemical and mechanical contributions in local adhesion force measurement with AFM: the specific case of polymers

Olivier Noel *, Maurice Brogly, Gilles Castelein, Jacques Schultz

Institut de Chimie des Surfaces et Interfaces (ICSI)-CNRS UPR 9069, Université de Haute Alsace (UHA), 15 rue Jean Starcky, BP 2488 Mulhouse Cedex, France

Received 14 July 2003; received in revised form 14 January 2004; accepted 20 January 2004

Abstract

The atomic force microscope (AFM) was used to perform surface force measurements in contact mode to investigate surface properties of model systems at the nanoscale. Two types of model systems were considered. The first one was composed of a rigid substrate (silicon plates) which was chemically modified by molecular self-assembling (SAMs) to display different surface properties (hydroxyl, amine, methyl and ester functional groups). The second system consists of model polymer networks (cross-linked polydimethylsiloxane or PDMS) of variable mechanical properties, whose surfaces were chemically modified with the same groups as before with silicon substrates. The comparison of the force curves obtained from the two model systems shows that the viscoelastic or mechanical contribution dominates in the adhesion on polymer substrates. Finally, a relationship, which expresses the separation energy at a local scale as a function of the energy dissipated within the contact zone, on one hand and the surface properties of the polymer on the other, was proposed.

Keywords: Adhesion; Adherence; Polymer; SAMs; AFM; Mechanical properties; Grafting

1. Introduction

The atomic force microscope (AFM) is a promising tool for the investigation of material surface properties at the nanoscale. Precise analysis of adhesive and mechanical properties, of chemically modified surfaces can be achieved with a nanometer scale probe. Thus, numerous studies on AFM characterization of surface properties are currently reported in the literature [1–4]. However, only few of them take into consideration both the chemical and mechanical contributions that are often simultaneously involved in surface force measurements with AFM.

The purpose of this study is to quantify the different contributions (adhesive and mechanical) that are involved in surface force measurements with AFM in order to establish the separation energy on one hand and, the surface and bulk viscoelastic properties on the other hand. As model substrates, we have used silicon wafers (or SAMs) and cross-linked PDMS sheets, which are both grafted with identical molecules to provide various surfaces. All AFM measurements reported here are performed with a silicon nitride tip (Si_3N_4), at ambient temperature, in air.

2. Experimental

2.1. Preparation of oxidized silica surface

Silicon wafers (1 0 0) (supplied by MAT TECHNOLOGY France) polished on one side were used as substrate for the SAM film grafting.

* Corresponding author. Tel.: +33-389-608-775; fax: +33-389-608-799.
E-mail address: o.noel@uha.fr (O. Noel).

0014-3057/$ - see front matter © 2004 Elsevier Ltd. All rights reserved.
doi:10.1016/j.eurpolymj.2004.01.014

Before grafting, the substrates are modified to produce a hydrophilic surface (SiO_2). The silicon surface was first cleaned with ethanol and dried with nitrogen before oxidation. Oxidized surfaces were obtained by immersing the cleaned substrates in a warm piranha (60 °C) solution (3:7 v/v 30% H_2O_2 and H_2SO_4 mixture) for about 30 min, and then thoroughly rinsed with deionized and twice distilled water. Just before grafting with organosilane molecules, the wafers are dried with nitrogen. This piranha treatment produces a high hydroxyl group density on the surface (SiOH groups), to which functional molecules will adsorb upon hydrolysis [5].

Surfaces modified with hydroxyl groups hereafter referred to as Si_{OH} were synthesized this way and immediately probed in order to avoid environment contamination of the highly reactive SiOH groups.

In this paper, Si_{wafer} refers to a silicon wafer previously cleaned in hexane then in ethanol in an ultrasonic bath. That means a contaminated layer (native oxide layer) still remains on the surface.

2.2. Functionalized SAMs preparation

Four organosilane molecules (supplied by ABCR Karlsruhe, Germany) were used for the elaboration of homogeneous model surfaces on the substrate. Two hydrophobic ones were prepared, using hexadecyltrichlorosilane ($C_{16}H_{42}O_3Si$ or Si_{CH3}) and 1H,1H,2H,2H-perfluorodecylmethyldichlorosilane ($C_{11}H_7Cl_2F_{17}Si$ or Si_{CF3}) and, two hydrophilic ones, using (6-aminohexyl)-aminopropyltrimethoxysilane ($C_{12}H_{30}N_2O_3Si$ or Si_{NH2}) and 2-(carbomethoxy)ethyltrichlorosilane ($C_4H_7Cl_3O_2Si$ or Si_{ester}). Our functionalized SAMs were prepared by vapour-phase self-assembling technique [6], which uses vapour deposition of the molecules onto the substrate. In this method, the oxidized silica surfaces are placed above a mixture of the organosilane (100 μL) in 3 mL mineral oil, which was previously de-gassed. The vapour-phase formation of the molecular film on the substrate is performed in a vacuum chamber (50 min at 5×10^{-3} Torr) at room temperature. The absence of solvent prevents the SAMs of a possible incorporation of small contaminant molecules and defects. Moreover, a previous study [7] showed that the molecular films prepared with this method, are more ordered.

2.3. Cross-linking and functionalization of PDMS

PDMS chains were previously cleaned in acetone in order to reduce the polydispersity index. PDMS samples were then cross-linked under nitrogen in a glove box using tetrakis(dimethylsiloxy)silane as a cross-linker and a platinum-based catalyst. Cross-linking was achieved by heating the samples at 80 °C for 12 h. Table 1 reports the PDMS substrate features before and after cross-linking. In particular, the classification of PDMS substrates refers to the entanglement mass after cross-linking. Thus, PDMS 0.8k is the highest modulus (or hardest) substrate, whereas 34k refers to the softest one.

Before grafting, as for silicon substrates, the PDMS substrates were chemically modified to produce a hydrophilic surface (SiO_2). The PDMS surfaces were first cleaned with toluene for five days and dried under vacuum before oxidation. Oxidized surfaces were obtained by using a water vapour plasma treatment (Plasma power: 80 W for 30 s). This treatment produces a high hydroxyl group density on the surface (SiOH groups), to which functional silanes will adsorb upon hydrolysis. Grafting procedure is the same as with silicon wafers (vapour-phase molecular self-assembling technique).

2.4. Characterization of the SAMs on wafer of silicon and cross-linked PDMS substrates

Contact angle measurement is an effective method to characterize surface hydrophilicity and hydrophobicity. Wetting properties with water and with TCP (TriCresylPhosphate) in a thermostated chamber (20 °C) are measured with a Krüss G2 system. The volume of the liquid drop in air lies between 1 and 2 μL and the measurement cell was previously saturated with the liquid vapour. Equilibrium static angles, advancing, and receeding angles for water and equilibrium static angles for TCP are reported in Table 2. We underline that for a given surface chemistry, the contact angles were independent of the nature of the underlying substrate (silicon wafer or cross-linked PDMS). Moreover, it is interesting to note that the correlation obtained between contact angle measurements and the hydrophobic–hydrophilic character corresponds to the one expected for the grafted surface groups. Moreover, the wetting hysteresis is

Table 1
Weight molecular mass (M_w in g mol^{-1}) and polydispersity index (I_p) before and after cleaning the PDMS chains in acetone, entanglement mass of cross-linked PDMS (M_c in g mol^{-1})

Classification	M_w before cleaning	M_w after cleaning	M_c	I_p before cleaning	I_p after cleaning
PDMS 0.8k	1500	1500	800	1.5	1.5
PDMS 13k	12,500	10,900	13,000	2	1.5
PDMS 34k	54,500	53,200	34,000	2	1.6

Table 2
Wetting properties for different surface chemistries with water and TCP

End groups	Water			TCP
	θ_e (°) ±2	θ_r (°) ±2	θ_a (°) ±2	θ_e (°) ±2
CF3	106	117	86	67
CH3	103	111	101	66
Si_{wafer}	78	81	70	47
PDMS	108			50
COOR	71	75	59	37
NH2	57	59	21	28
OH	6			25

θ_e is the equilibrium static angle, θ_r is the receeding angle and θ_a is the advancing angle.

low (except with the Si_{CF3} and Si_{NH2} surfaces). This means that our functionalized surfaces show high compacity and homogeneity at macroscopic scale. Finally, PDMS and silicon substrates have the same wetting properties with the TCP (apolar liquid).

Surface morphologies of the different types of layers were studied by AFM (Nanoscope III-Digital Instrument) in the TappingMode™ and in the Contact Mode AFM (for PDMS substrates) (see Fig. 1). SAMs topographic and phase contrast AFM images (image size: 500 nm × 500 nm) confirmed that no aggregates were formed and showed a complete homogeneous recovery of the grafts (at a local scale). Moreover, the RMS roughness of 0.15 nm for silicon wafer substrate and 0.3 nm for PDMS substrates deduced from the AFM images, which were the expected value for the substrate roughness, confirmed that our grafts were well ordered and packed at micrometer scales (this is also the case for the Si_{CF3} and Si_{NH2} surfaces). It also confirms that the piranha or plasma treatments (in optimised conditions) have no effect on the roughness of the substrates.

XPS spectrometry (Leybold LHS 11) with a take-off angle of 15° was also carried out. Comparison of the spectra related to the different types of molecules grafted on the silicon wafer with the spectra obtained on the silicon wafer confirms the effective grafting. Moreover, no peaks related to the chloride element have been detected in reference to the spectra of the neat chlorinated molecules. This confirms the efficiency of the grafting reaction and of the surface cleaning procedure.

The thickness of the oxide and organic films were determined by ellipsometry measurements by fitting both the refractive index and the thickness of the film (Table 3).

These results are coherent with the literature for the CH_3 and the NH_2 grafted films [8,9], and confirm that only one monolayer was grafted in these cases. These thicknesses were determined by initially measuring and substracting the thickness of the oxide layer formed during the piranha treatment. A 3 nm reproducible value was obtained.

Even though important efforts were made to characterize the grafted surfaces (XPS, ellipsometry, wetting, AFM images), one can suspect that the grafting density and the morphology of the monolayer may affect the comparison of these surfaces in terms of quantitative adhesion force. To prevent such effects, evolution with grafting time of the properties of the monolayers was

Table 3
Ellipsometry measurements

End groups	Film thickness (Å)	Theoretical film thickness
CF3	12	14
CH3	21	22.5
COOR	5	6
NH2	9	15

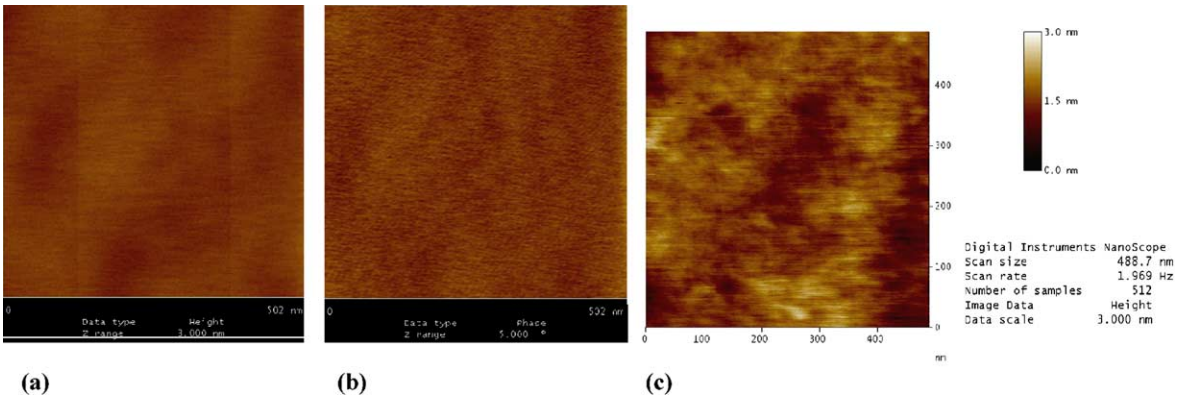

Fig. 1. (a) and (b) Topographic and phase AFM images of CH_3 SAMs grafted on a silicon wafer (TappingMode™, image scale: 500 nm × 500 nm, height and phase scale 3 nm and 5°); (c) Topographic image of CH_3 SAMs grafted on a PDMS substrate (Contact mode, image scale: 500 nm × 500 nm, height 3 nm).

PDMS	Elasticity Domains (%)	Deformation at break (%)	Young modulus (MPa)
0.8k	40	196	2.2
7k	46	210	0.6
13k	47	250	0.3
34k	52	250	0.1

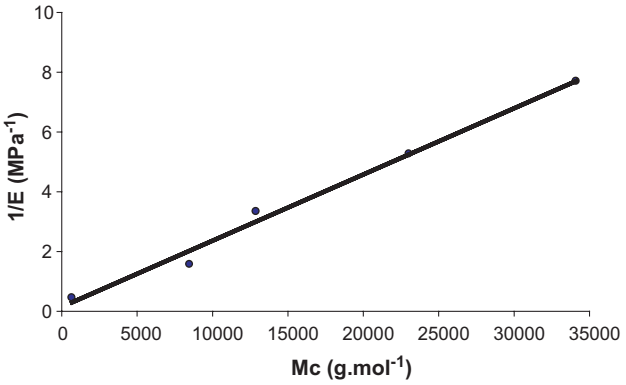

Fig. 2. Mechanical properties of the cross-linked PDMS. The curve $1/E = f(M_c)$ shows that Flory theory is verified (E is the Young's tensile modulus determined with a 1 mm/min strain rate and M_c is the entanglement mass).

investigated in previous studies [10]. In the present study, grafting time has been chosen to get stable layers versus time.

Finally, macroscopic mechanical tests (uniaxial elongation and dynamical tests) were carried out on PDMS substrates and were found to follow the Flory theory [11] of rubberlike elasticity (Fig. 2). This shows that the preparation process of the PDMS produces samples of well-controlled macroscopic mechanical properties (this is also confirmed by the reproducibility of the measurements). Moreover, dynamic mechanical tests have shown that the Young's modulus is independent of the deformation rate within the experimental conditions. Finally, we also checked that the plasma treatment does not affect the mechanical properties of the studied PDMS substrates.

3. Force–distance curves and AFM calibration

3.1. Force–distance curves

Force measurements with AFM, in the contact mode, consist in detecting the deflection of a spring (or cantilever) bearing a nitride silicon tip at its end, when interacting with the sample surface. The deflection of the cantilever is detected by an optical device (four quadrants of photodiodes) while the tip is vertically moved forward and backward thanks to a piezoelectric ceramic (or actuator). Thus, one can obtain a deflection–distance (DD) curve. Moreover, provided the spring constant of the cantilever (k_{tip}) and the vertical deflection (Δz) are known, we can calculate the force (F) by using Hooke's law:

$$F = k_{tip} \cdot \Delta z$$

The DD curves were performed in the air with an available commercial apparatus (NanoscopeIIIa D3000, DI). A schematic representation of a DD curve obtained when probing a hard surface is reported in Fig. 3, on which we can distinguish different zones. In zone A, the cantilever is far from the surface and stays in a state of equilibrium (no interaction with the surface). The cantilever deflection is zero. During the approach toward (or withdrawal from) the surface, the tip interacts with the sample and a jump in (or jump-off) contact occurs (zones B (for loading) and F (for unloading)). These instabilities take place because the cantilever becomes mechanically unstable. Usually, for rigid surfaces, because of these mechanical instabilities, the jump-in contact is not significant enough to determine attractive Van der Waals forces. However, the adhesion force ($F_{adhesion}$) between the tip and the sample is directly related to the jump-off ($\Delta z_{jump\text{-}off}$) by Hooke's relation, assuming an elastic regime:

$$F_{adhesion} = k_{tip} \cdot \Delta z_{jump\text{-}off}$$

When in contact, the cantilever deflection is equal to the piezoelectric ceramic displacement provided no indentation of the substrate occurs (zones C (for loading) and D (for unloading)). A rigid reference sample (cleaned silicon or cleaved mica) is used to scale the DD curve in deflection by fixing to unity the slope value of the contact line.

3.2. AFM calibration

One of the fundamental points to obtain reproducible, quantitative and reliable data is the calibration procedure, which should be rigorous and systematic for all measurements. In particular, the spring constant of the cantilever has been determined by using a non-destructive method, based on the use of reference rectangular cantilevers [12]. The cantilever used in this study was a triangular shaped cantilever (supplied by Nanosensor-Germany) and had an effective 0.30 ± 0.03 N m^{-1}

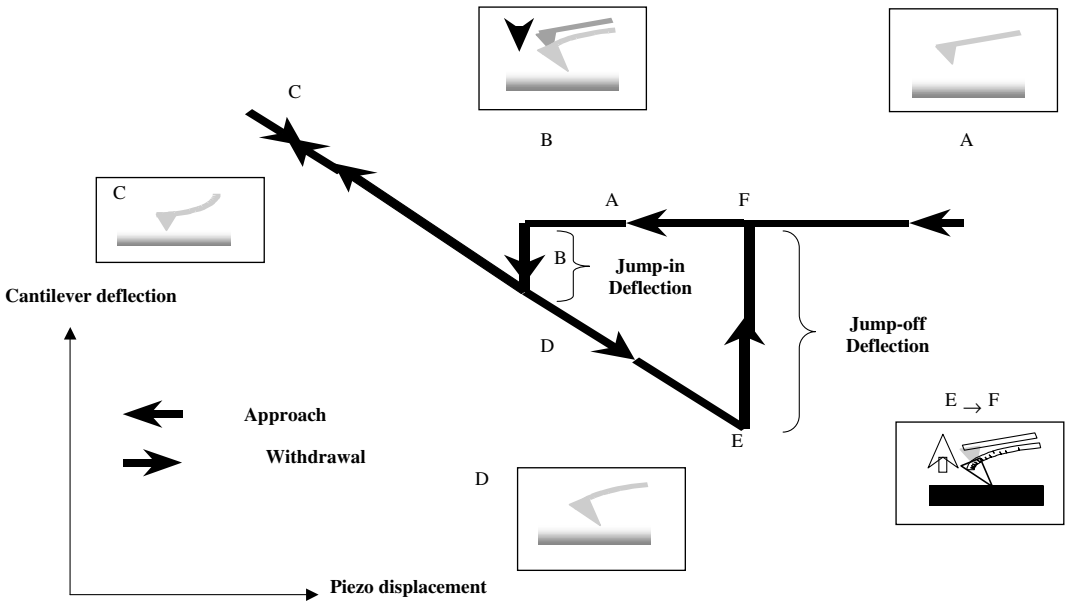

Fig. 3. Schematic representation of a DD curve.

spring constant. This value is similar to the one determined by the thermal fluctuation measurement method [13].

To deduce works of adhesion from our experimental values, it was also necessary to have a good estimation of the radius of the probe and thus of the tip–sample contact area. For convenience, we deduced the radius on the basis of the shape revealed on a MEB picture taken at the end of the AFM measurements. Another experimental technique of tip radius estimation using nanoindentation experiments on a model polymer (perfectly elastic) has also been used [14]. Fig. 4 shows that the force versus the indentation depth curve evolves according to two regimes. In our case, the transition between the two modes corresponds to the change in the contact geometry (sphere–plane contact to cone–plane contact). The observed transition shows that our tip radius can be estimated to 50 nm ± 5 nm. Comparison of the two methods gives the same tip radius.

Other instrumental features have to be taken into account. In particular, the non-linearity of the optical detector is the consequence of a non-homogeneous spreading of the laser spot on the detector. This non-linearity has been studied by reporting the slope of the contact line (zones C or D) of a DD curve (obtained on a hard surface and considering that there is no non-linearity at the middle of the photo detector) versus the tension (V) measured by the detector. The domain of linearity of the detector appeared to lie between ±2 V. If non-linearity is not taken into account, the error on the quantitative results can be preponderant. All our measurements were done in the linearity domain of the detector.

We have also studied the actuator, which shows a hysteresis and a non-linearity in its vertical displacement. Considering that our actuator was thermally stable, we have reported the slope of the contact zones (zones C and D) versus the amplitude of the contact zone and the scan speed. We have observed that a discrepancy appears for very low scan speed (60 nm s^{-1}), whereas for higher scan speed (18 μm s^{-1}), the viscosity of the environment could be significant. A speed of about 6 μm s^{-1} is a good compromise for our actuator.

In addition, checking regularly and randomly the adhesion force on a reference silicon wafer verifies the contamination of the tip during the measurements. When the tip is contaminated, a new tip is used and characterized. In that way, we can select tips with about the same radius and the same spring constant in order to compare the experimental values. We might also mention that tip contamination occurs a few times in comparison with the great number of realized DD curves.

If we consider that the main uncertainties in a pull-off force measurement with AFM are due to the determination of the spring constant and the radius of the tip, we can approximate an error of 10% on the measurement of an adhesion force (due to the uncertainty of the method of calibration of the tip), and a relative error of 20% on the determination of the work of adhesion and surface tensions (due to a 10% error on the determination of the tip radius). The uncertainty on the tip radius is evaluated on the basis of nanoindentation experiments

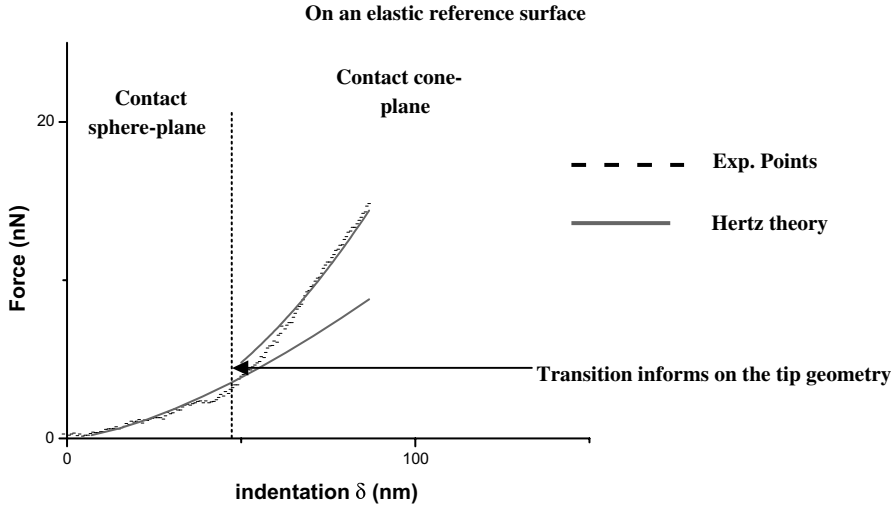

Fig. 4. Experimental determination of the tip radius. Indentation curve of a reference elastic surface.

with such a tip on elastic polymer network. Nevertheless, even if 20% error appears high, one must consider this error as a systematic error. Indeed, all measurements (about 100 for a given surface) were performed with a tip with the same characteristics (tip radius and cantilever stiffness). Thus, experimental results are significant and the contribution of the different grafts can be discriminated.

4. Results and discussion

4.1. DD curves from rigid systems of controlled surface chemistry

The tip–sample interaction force was first measured on chemically modified SAMs obtained on rigid substrates (silicon wafers). Fig. 5 shows that AFM measurements in our conditions are sensitive and significant to a chemical modification of the layers. When jump-off contact occurs, we measure the corresponding pull-off deflection. Pull-off deflection values, hereafter referred as Δz_{po}, increase in the following order:

$$\Delta z_{poSiCF3} < \Delta z_{poSiCH3} < \Delta z_{poSiwafer} < \Delta z_{poSiester} < \Delta z_{poSiNH2} < \Delta z_{pofSiOH}.$$

Knowing the pull-off deflection one can easily deduce the adhesion force, if the cantilever spring constant k_{tip} is known ($F_{adhesion} = k_{tip} \cdot \Delta z_{po}$). Thus the adhesion force value increases with the hydrophilicity of the surface. However, the measured adhesion force depends strongly on the tip–sample contact area e.g. on the tip radius in the case of rigid substrates. Sugawara et al. [15] suggested that the adhesion force is proportional to the tip radius. This is the reason why we have normalized our values by dividing the adhesion forces measured by a given tip with the adhesion forces of the Si_{CF3} sample corresponding to the same tip. The choice of normalization upon Si_{CF3} has been done considering that Si_{CF3} is

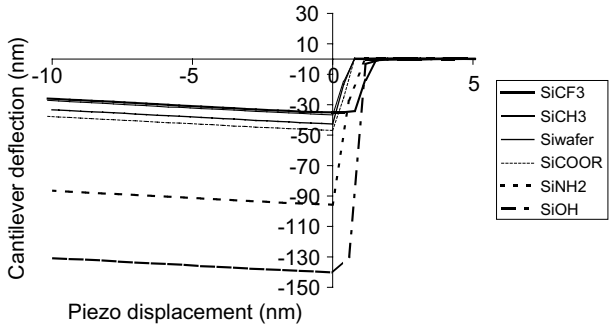

Fig. 5. Experimental DD curves on functionalized silicon wafer.

the most hydrophobic surface. In that way, we prevent ourselves from the knowledge of the geometrical aspect of the tip. A thermodynamic work of adhesion (W_0) can be calculated from the DMT theory [16] by using the following relationship:

$$W_0 = -\frac{F_{adh}}{2\pi R} \quad (1)$$

F_{adh} is the adhesion force and R is the tip radius.

From this expression, we can deduce AFM normalized W_0 from the experimental normalized adhesion forces. In the following, an attempt is made to correlate the experimental AFM thermodynamic works of adhesion calculated from relation (1) and measured wetting properties of the investigating systems. A basic requirement to be satisfied is the similarity of the intermolecular forces that operate across the interface, in both wetting and adhesion force measurements. Since, the AFM measurements involve the contact of a polar material (Si_3N_4 tip) with the substrate, we have chosen to use for the wetting experiment, a polar liquid (water) that exchanges similar intermolecular forces with the substrate, as does the tip in adhesion. Fig. 6 shows that normalized W_0 decreases linearly (correlation factor is 0.99) with the contact angle measured with a water droplet or increases linearly with the hydrophilicity of the surfaces. Nevertheless, singularities are observed for Si_{NH2} and Si_{OH} surfaces (very hydrophilic surfaces). But, considering that the measurements are performed in air, a capillary bridge is formed for these very hydrophilic surfaces and the pull-off mechanism could be different from the other surfaces [14,17]. This could explain why the corresponding point for Si_{NH2} and Si_{OH} (in Fig. 6) does not fit the linear extrapolation.

4.2. DD curve measurements: the specific case of polymers

Fig. 7 shows the DD curves obtained on a silicon substrate on one hand, and on a PDMS substrate on the other hand. The comparison of the shape of both

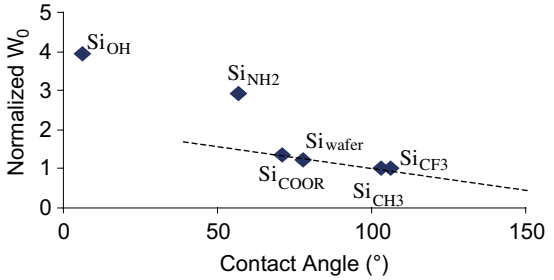

Fig. 6. AFM normalized thermodynamic works of adhesion deduced from the DMT theory versus the contact angles determined with water.

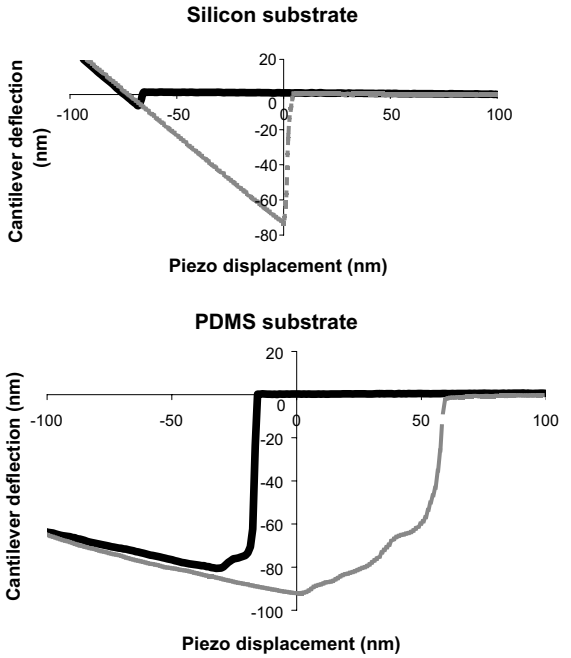

Fig. 7. Comparison between a DD curve obtained on a silicon substrate (top) and a PDMS substrate (bottom).

curves clearly shows the significant contribution of the mechanical properties of the polymer. In particular, compared to silicon wafer, the jump-off contact occurs over a large piezo displacement scale and could correspond to a progressive dewetting of the tip by polymer chains during retracting. The jump-off amplitude is also higher than for silicon wafer. This means that we measure the adherence rather than the adhesion on a polymer substrate. Adherence includes both chemical and mechanical contributions, whereas adhesion is defined by the intermolecular interactions.

The comparison also shows that the absolute values of the loading and unloading slopes in the DD representation are much lower than unity in the case of soft polymer systems.

The jump-in amplitude is also more important for a polymer and cannot be attributed to an instability of the tip only. To explain this feature, we have investigated different assumptions including creep and the formation of a polymer nanoprotuberance during the approach cycle. Currently, none of these assumptions have clearly explained this effect (no creeping is observed for our substrates and the nanoprotuberance appears too small) [18]. Thus, in a first approximation, the beginning of the indentation is assumed to be at the minimum of the DD curve.

Influences of creep effects on the AFM measurements have also been investigated. In Fig. 8, we have reported AFM creep experiments [19] on two different PDMS

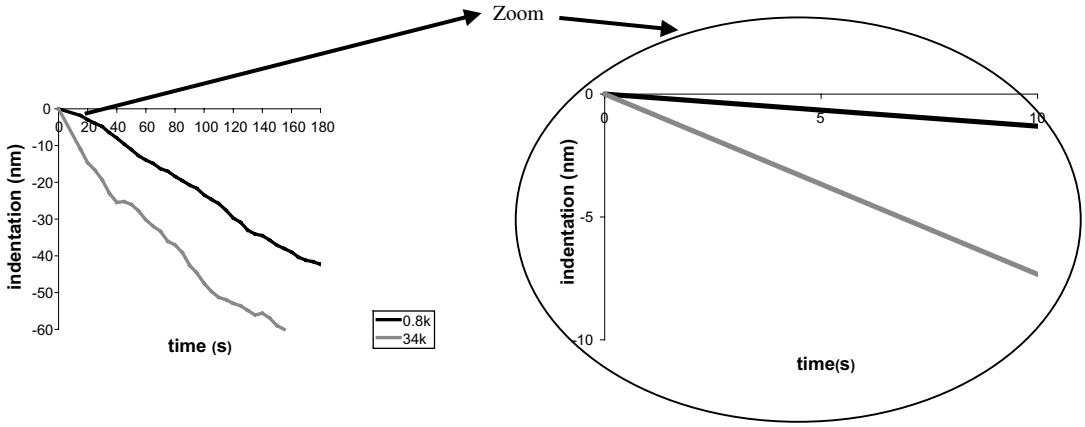

Fig. 8. Creep experiments with the AFM (corrected from thermal drift) on the 0.8k and 34k PDMS networks.

substrates (PDMS 0.8k and PDMS 34k). Obviously, considering the experimental contact time ($t_{exp} < 0.1$ s), the creep effect is not significant in our force curve measurements.

4.3. Force–indentation curves (F–I curves) deduced from DD curves

Before monitoring DD curves on PDMS, the actuator and the cantilever were thermally stabilized. The laser spot in contact with the tip was positioned in such a way that tangential forces, due to frictional forces, were minimized. We carried out these measurements on the basis of the above prerequisites so that force measurements could be liable and compared. *F–I* curves (Fig. 9) are deduced from DD curves by assuming that for a given force, the indentation depth is the difference between the experimental deflection value (ds) and the one that should be observed if the material was rigid (dr deduced from the slope of 1 for rigid materials).

In our experiments, we have also taken care to ensure that we have really indented the polymer. Thus, considering the normal stiffness of the cantilever, it is possible to determine the maximal indentation depth (δ_{max}), using the following relationships:

$$k_{tip} = 2 \times E^* \times \sqrt{(R\delta_{max})}$$

k_{tip} is the constant stiffness of the cantilever, E^* is the reduced modulus and R is the tip radius. The maximal indentation depths are reported in Table 4.

For the hardest substrate, the maximal indentation depth is estimated to be 89 nm. Thus, whatever is the polymer substrate, all our AFM measurements are done at a constant 80 nm indentation depth. Finally, the longitudinal stiffness of the cantilever (k_x), sliding can occur before indenting the polymer. Nevertheless, sliding effect is assumed negligible compared to the total indentation depth.

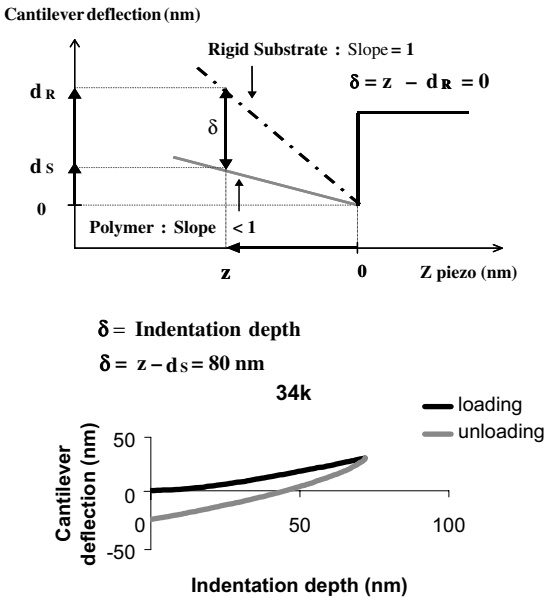

Fig. 9. Schematic representation to determine *F–I* curves from DD curves (left) and characteristics experimental *F–I* curves on PDMS 34k.

Table 4
Calculation of the theoretical maximum indentation depth of the tip for our polymer networks

PDMS	Maximal indentation depth
0.8k	90
13k	5000
34k	27,000

Table 5
Ratio $\left(\frac{F_{adh}PDMSX}{F_{adh}SiX}\right)$ for CH_3, NH_2 and as received substrates and for three PDMS of different mechanical properties

	Given grafting ↓					
End group Raw material	$\frac{F_{PDMS}}{F_{Si}}$	End group CH_3	$\frac{F_{PDMS}}{F_{Si}}$	End group NH_2	$\frac{F_{PDMS}}{F_{Si}}$	
0.8k/Si	1.1	$0.8k_{CH3}/Si_{CH3}$	1.0	$0.8k_{NH2}/Si_{NH2}$	1.2	
13k/Si	1.8	$13k_{CH3}/Si_{CH3}$	1.5	$13k_{NH2}/Si_{NH2}$	1.5	
34k/Si	2.0	$34k_{CH3}/Si_{CH3}$	1.9	$34k_{NH2}/Si_{NH2}$	2.2	← Given substrate

4.4. DD curves on systems of controlled surface chemistry and controlled mechanical properties

We have realised AFM measurements on cross-linked PDMS substrates with different Young's modulus and grafted with the same molecules as for the silicon wafers before (CH_3 and NH_2 SAMs). All DD curves obtained on polymers have been done at the same indentation depth, as discussed previously. In order to compare the adhesion forces obtained from the different substrates, we have considered the following ratios: $\left(\frac{F_{adh_{PDMSX}}}{F_{adh_{SiX}}}\right)$ ($F_{adh_{PDMS}}$ and $F_{adh_{Si}}$ represent the adhesion force measured on respectively PDMS and silicon substrates and X represents the functionality of the grafting).

Table 5 shows that for a given PDMS substrate (for example, 0.8k) or a given Young's modulus, the ratios are independent of the surface chemistry, whereas for a given grafting, the ratios are dependent on the mechanical properties of the substrate. Thus, for a given substrate, we have the following expression:

$$F_{adh_{PDMSX}} = F_{adh_{SiX}} \times \phi \quad (2)$$

ϕ is a constant dependent on the mechanical properties of the substrate.

However, for a rigid substrate, the DMT theory gives:

$$F_{adh_{SiX}} = -2\pi R W_0 \quad (3)$$

R is the tip radius and W_0 is the thermodynamic work of adhesion.

By replacing (3) in (2), we get:

$$F_{adh_{PDMSX}} = -2\pi R W_0 \times \phi \quad (4)$$

By introducing a dimensional constant ($k' = (2\pi R)^{-1}$), we get an energy of separation, $G_{adh_{PDMSX}}$ that can be expressed as follow:

$$G_{adh_{PDMSX}} = W_0 \times \phi \times 2\pi R \times k'$$

or

$$G_{adh_{PDMSX}} = W_0 \times \phi(M_c, T) \quad (5)$$

G is the separation energy and $\phi(M_c, T)$ is a viscoelastic dissipative function dependent on the network molecular structure (M_c) and on the temperature (T).

Table 6
Average viscoelastic dissipation function deduced from Table 5

PDMS substrates	$\phi(v = 10$ Hz, $T = 20°)$
0.8k	1.1 ± 0.1
13k	1.6 ± 0.2
34k	2.0 ± 0.2

This relationship clearly expresses the mechanical contribution from the chemical one in a force curve measurement with AFM. According to Table 5, $\phi(M_c, T)$ is determined for each substrate for a given speed and a given temperature, and ϕ is independent of the surface chemistry. Moreover, the experimental ϕ values, reported in Table 6, are coherent. Indeed, $\phi(M_c, T)$ cannot theoretically be lower than 1 (the limit value which corresponds to a zero separation speed) and should increase, while the Young's modulus decreases (which means that energy dissipation in the bulk is higher when the network is softer). Moreover, even if the dependence of ϕ on the separation speed v is not dominating in the range of the available rates with the AFM, it is obvious from the F–I curves in Fig. 9 that dissipation occurs for the 34k sample and that this dissipation is included in the dissipative function ϕ.

5. Conclusions

This study has shown that a rigorous experimental procedure and AFM calibration is necessary to get quantitative values with the AFM. From then on, it is possible to determine in situ thermodynamic works of adhesion at a local scale with the AFM. In particular, provided no capillary force contributions are involved in the adhesion mechanism, thermodynamic works of adhesion linearly increase with hydrophilicity of the surfaces. Finally, we have compared two model systems with similar surface chemistry properties but with different mechanical behaviour (silicon wafer and PDMS substrates). This allowed us to express and quantify the mechanical and chemical surface contributions in a force curve measurement. From then on, we have established a relationship of the separation energy at the nanoscale that decouple both intermolecular and mechanical contributions.

Acknowledgements

Authors are grateful to C. Frétigny, H. Haidara and K. Mougin for their fruitful discussions.

References

[1] Gauthier S, Aime JP, Bouhacina T, Attias AJ, Desbat B. Langmuir 1996;12:5126–37.
[2] Schonherr H, Hruska Z, Vancso GJ. Macromolecules 2000;33:4532–7.
[3] Bar G, Brandsch R, Whangbo MH. Langmuir 1998;14: 7343–7.
[4] Grinevich O, Mejiritski A, Neckers DC. Langmuir 1999; 15:2077–9.
[5] Mougin K, Haidara H, Castelein G. Colloids Surf Physicochem Eng Aspects 2001;193:231–7.
[6] Chaudhury MK, Whitesides GM. Science 1992;255:1230–2.
[7] Vonna L. Thesis, Mulhouse, France, 1999.
[8] Mougin K. Thesis, Mulhouse, France, 2001.
[9] Wood J, Ravi S. Langmuir 1994;10:2307–10.
[10] Elzein T, Brogly M, Schultz J. J Surf Interf Anal 2003: 35.
[11] Ferry JD. Viscoelastic properties of polymers. John Wiley and Sons, Inc.; 1980.
[12] Gibson CT, Weeks BL, Lee JRI, Abell C, Rayment T. Rev Sci Instrum 2001;72:2340–3.
[13] Levy R, Maaloum M. Nanotechnol Bristol 2002;13:33–7.
[14] Noel O, Brogly M, Castelein G, Schultz J. In: MRS Proceedings, vol. 778, San Francisco, 2003.
[15] Sugawara Y, Ohta M, Konishi T, Morita S, Suzuki M, Enomoto Y. Wear 1993;168:13–6.
[16] Derjaguin BV, Muller VM, Toporov YP. J Colloid Interf Sci 1975;53:314.
[17] Noel O, Brogly M, Castelein G, Schultz J. Langmuir, in press.
[18] Aime JP, Michel D, Boisgard R, Nony L. Phys Rev B: Condens Matter 1999;59:2407–16.
[19] Basire C, Fretigny C. EPJ Appl Phys 1999;6:323–9.